IN- SITU INFRARED MEASUREMENTS OF FREE-FLYING SILICATE DURING CONDENSATION IN THE LABORATORY

Shinnosuke Ishizuka[1,2], Yuki Kimura[1], and Itsuki Sakon[3]

[1] Institute of Low Temperature Science, Hokkaido University, Hokkaido Sapporo 060-0819, Japan

[2] Department of Earth Science, Graduate School of Science, Tohoku University, 6-3 Aramakiaza-Aobu, Aoba-ku, Sendai 980 8578, Japan

[3]Department of Astronomy, School of Science, University of Tokyo, 7-3-1 Hongo, Bunkyo-ku, Tokyo 113-0033, Japan

Abstract

We developed a new experimental system for infrared (IR) measurements on free-flying nucleating nanoparticles *in situ*, and applied it to studies on silicate particles. We monitored the condensation of magnesium-bearing silicate nanoparticles from thermally evaporated magnesium and silicon monoxide vapor under an atmosphere of oxygen and argon. The IR spectrum of newly condensed particles showed a spectral feature for non-crystalline magnesium-bearing silicate that is remarkably consistent with the IR spectrum of astronomically observed non-crystalline silicate around oxygen-rich evolved stars. The silicate crystallized at <500 K and eventually developed a high crystallinity. Because of the size effects of nanoparticles, the silicate would be expected to be like a liquid, at least during the initial stages of nucleation and growth. Our experimental results therefore suggest decreasing possible formation temperature of crystalline silicates in dust formation environments with relatively higher pressure.

KEYWORDS: dust; infrared: stars; methods: laboratory: molecular; methods: laboratory: solid state

1. INTRODUCTION

Silicate dust is one of the most abundant minerals in the universe, and is widely distributing in shells around evolved stars (Waters et al., 1996; Molster et al., 2002; Jones, et al., 2012), disks around young stars (Bouwman et al., 2001, van Boekel et al.,2005, Honda et al. 2006), comets (Hanner et al., 1994, Watanabe et al., 2009), and so on. The 10-μm band feature with a wavelength range of 8 μm to 12.5 μm, arising from Si–O stretching vibrations, holds information on unrevealed evolutionary processes of silicate dust. Data from the Infrared Space Observatory mission revealed the existence of crystalline silicates around evolved stars from the profile of their IR band features, which was mainly attributed to amorphous silicate with contributions from various amounts of crystalline silicate. Molster & Kemper (2005) concluded that 10–15 % of crystalline silicates are present in the outflows of asymptotic giant branch (AGB) stars with high mass-loss rates.

Numerous laboratory experiments aimed at reproducing the observed spectra by direct condensation (e.g., Tsuchiyama 1998; Kimura et al., 2009) or by annealing of amorphous silicates (e.g. Hallenbeck et al., 2000; Murata et al., 2009; Kimura et al., 2011a) have produced IR spectra with variations caused by various factors, including crystallinity, chemical composition, temperature, size, and shape. However, in the case

of transmittance IR spectra, candidate particles are dispersed in a KBr medium that has destructive effects on the polarization of the particles (called the "medium effect"), and the agglomeration of particles leads to diversification in some IR band features, such as the peak position, full-width of half maximum (FWHM), and relative intensity (Bohren & Hufman 1983). Some studies have predicted a diversification in the 10-μm band structure of Mg-bearing silicates in KBr media by means of calculation (Jäger et al., 1998; Fabian et al., 2001; Koike et al., 2010). Recently, attempts have been made to extract more-detailed information, such as the magnesium–iron ratio and the temperature of silicate particles, from the fine structure of the IR features (Fabian et al., 2001). In these cases, the effects of the medium in which the spectra are recorded must be eliminated to permit direct comparison with astronomical observations. We have therefore developed a new experimental system to permit recording of transmittance IR spectra of nanoparticles *in-situ* during nucleation and growth of model dust particles without the embedding effects of KBr; we named this system the Free-flying In-situ infrared measurement of Nucleating nanoparticle Experimental (FINE) system. To investigate the formation process of silicates around evolved stars, we monitored the IR spectra of silicate nanoparticles formed by homogeneous nucleation from a thermally evaporated hot vapor by using our FINE system, and directly compared the

laboratory-generated spectra with astronomical spectra.

2. EXPERIMENTAL PROCEDURE

Silicate particles were produced in a specially designed vacuum chamber attached to a Fourier-transform IR (FT-IR) spectrometer (Fig. 1). The original chamber was made of stainless steel with two windows to provide an optical path for FT-IR consisting of KRS5 (thallium bromoiodide), which has a high transmittance in the mid-IR region and shows no cleavage. The inner diameter of the chamber was 9 cm, and the height of the chamber where the dust-model nanoparticles were produced was 20 cm. The cylinder of the chamber was connected to a turbo molecular pump (50 L/s) to permit evacuation. When the pressure in the chamber had fallen to below 1×10^{-4} Pa, the gate valve was closed and high-purity O_2 (99.9%) and Ar (99.9999%) were injected. Initially, the pressure was raised to $3.0 \pm 0.5 \times 10^2$ Pa with O_2 gas, and then it was raised to a total pressure of 1.0×10^4 Pa with Ar. The gas pressure was measured by means of a capacitance manometer (ULVAC, GM-1000). The evaporation source was a V-shaped Ta boat (30 mm in length, 5 mm in width, and 0.03 mm in thickness, with a purity of 99.95%); this was connected to Cu electrodes to permit rapid electrical-resistance heating to 2200 ± 200 K. The source temperature was monitored by using a radiation

thermometer (λ = 0.8−1.6 μm; FTZ2, Japan Sensor Co). Several tens milligram of Mg (99.9% pure) and SiO powder (99.95% pure) on the evaporation source were thermally evaporated. The resulting gas flowed upward due to thermal convection generated by the evaporation source and then it cooled to induce homogeneous nucleation of nanoparticles, which became visible as a smoke. An optical path for FT-IR just above the evaporation source permitted measurement of the IR spectra of the nascent condensate. A series of experiments were carried out under the regulated atmosphere while the height of the measurement position above the evaporation source was changed from 1 cm to 4, 6, 8 and 10 cm. The diameter of the IR beam was 2 cm at the measurement point. The resolution of the FT-IR spectrometer was 2 cm^{-1}. The flowing nanoparticles were captured by a collector fixed 10.5 or 18 cm above the evaporation source for the measurement at 1-8 cm or 10 cm, respectively, from the evaporation source. The collected particles were picked up by an amorphous thin film of carbon mounted on a standard copper grid for transmission electron microscopy (TEM). The produced particles were observed by TEM (Hitachi H-8100 or JEOL JEM-2100F) at an acceleration voltage of 200 kV. Particles from the collecting holder were agitated with KBr powder, which was used to prepare pellets by the conventional method for subsequent FT-IR observation.

3. RESULTS

We analyzed the metamorphosis of the Mg-bearing silicate particles by studying the 10-μm band in their IR spectra. Figure 2 shows typical 10-μm-band IR spectra of Mg-bearing silicate particles obtained by the FINE system at various heights above the evaporation source, which was heated to 2200±200 K. The 10-μm band obtained at observation heights of 1 and 4 cm has a broad feature at 9.7 μm, attributed to amorphous silicate with a Mg-rich composition. On the other hand, the spectra recorded at 6, 8 and 10 cm showed double-peak crystalline features, typical of forsterite. The left-hand band starting at about 9.7 μm was named the shorter-wavelength band, and the right-hand band arising at about 10.8–10.9 μm was named the longer-wavelength band. After the experiments, the produced particles were embedded in KBr pellets, and their IR spectra were recorded (Fig. 3); their size, shape, and crystalline structure were also determined by means of TEM (Fig. 4). The TEM analysis showed the presence of spherical particles with a diameter of 30–150 nm, together with a minor fraction of small cubic particles. The mean diameter of the spherical particles was 90.3 nm. Electron-diffraction patterns of the spherical and cubic particles were consistent with those of forsterite and MgO, respectively [Fig. 4(b)]. Although electron-beam

irradiation during the TEM observations induced deposition of contaminants and damage to the particles, as shown in Fig. 4(a), the alteration of the external shape of the particles was negligible, and the electron-diffraction patterns contain structural information on the nascent particle, because these were obtained before the bright-field image was recorded.

4. EFFECTS OF EMBEDDING IN POTASSIUM BROMIDE

Figure 3 shows the infrared spectrum of the Mg-bearing silicate nanoparticles obtained by the FINE system at a recording point 10 cm above the evaporation source together with the corresponding spectrum of the sample which was collected at 10.5 cm embedded in a KBr pellet. IR band features such as the peak wavelength, FWHM, and relative intensity for the collected nanoparticles embedded in KBr differed from those of the free-flying Mg-bearing silicate nanoparticles. The wavelengths of both the longer-wavelength and shorter-wavelength peaks were shifted by about 0.1 μm toward a longer wavelength after embedding in the KBr medium. This shift in the peak positions had been predicted by theoretical calculations using optical constants obtained from reflectance spectra (Fabian et al., 2001; Koike et al., 2010). Our new method succeeded in confirming that a shift in peak positions does indeed occur in the conventional

method using KBr pellets; Tamanai et al. (2006) have also demonstrated a shift in peak position to a longer wavelength as a result of a medium effect by using an aerosol technique with micrometer-sized forsterite particles having elliptical and irregular shapes. Our spherical nanoparticles showed the longer wavelength band with a peak at 10.8–10.9 μm, which is the first report for spherical nanoparticles and is consistent with the spectrum predicted by theoretical calculations (Fabian et al., 2001; Koike et al., 2010). The position of the peak of the longer wavelength band is more sensitive to chemical composition and is therefore a significant indicator of the concentration of iron (Fabian et al., 2001). To estimate the concentration of iron in silicate dust particles from astronomical spectra, a shift of ~0.1 μm is taken as corresponding to about a 25% addition of iron instead of magnesium (Fabian et al., 2001). We will record the free-flying IR spectra of iron-containing silicate (i.e., olivine) in future work and discuss carriers for iron in astronomical environments.

5. NUCLEATION AND GROWTH PROCESSES OF SILICATE PARTICLES

The relative intensity of the forsterite double bands at shorter and longer wavelengths varies with the annealing temperature of the amorphous silicate and it depends on the degree of crystallinity (Hallenbeck et al., 2000; Koike et al., 2010).

Forsterite samples annealed at higher temperatures, and therefore having higher degrees of crystallization, show more-intense longer-wavelength bands. This previously identified difference in the relative intensities of the peaks as a result of a difference in crystallinity can be applied to this study and illustrated our experiments. Newly condensed particles are carried upward by thermal convection, and subsequently crystallize gradually, as shown in Fig. 2. In particular, a sudden crystallization was observed at a height of between 6 and 10 cm [between Fig. 2(c) and Fig. 2(e)]. We evaluated the amount of crystalline forsterite that was present by fitting the measured spectra at each height from the evaporation source to spectra of amorphous silicate (Min et al., 2007) and crystalline silicate (Fabian et al., 2001), on the assumption that amorphous silicate and crystalline silicate were individually present. Spectral fitting revealed only <1% of crystalline silicate was present at 1–6 cm, as much as ~10% of crystalline silicate was present at 8 cm above the evaporation source, and more than 20 % at 10 cm. Lower crystallinity compared with the physical appearance of the crystalline feature is a result of significant difference in mass absorption coefficients between amorphous (2200 cm^2 g^{-1}) and crystalline (13000 cm^2 g^{-1}). But we can see crystallization proceeding efficiently at 6-10 cm region.

There are at least four possibilities to explain the increase of crystallinity shown by

1 the IR feature: direct nucleation of forsterite from residual vapor, oxidation of nuclei,
2 annealing of amorphous particles and secondary nucleation from molten particles.
3 First, direct nucleation of forsterite particles from residual vapor is unfavorable.
4 Condensation of silicates was confirmed within 1 cm above the evaporation source at
5 significantly high supersaturation. In that case, generally, evaporated vapor can be
6 exhausted by nuclei immediately due to very high growth rate compared with the
7 convection velocity of the rising vapor (10-15 cm/s) and then the partial pressure of the
8 remaining evaporant is negligible due to very low equilibrium vapor pressure (Kimura
9 et al. 2011c). Therefore, additional condensation to form new particles does not occur
10 above 1 cm, i.e., there is no possibility of direct condensation of crystalline silicate at
11 6-10 cm.
12 Secondly, we discuss oxidation of Mg and SiO used as starting material into MgO
13 and SiO_2 and its effects on crystallization. When experimental powders of Mg and SiO
14 evaporate, these molecules are oxidized by surrounding O_2 atmosphere during
15 nucleation. Though equilibrium vapor pressure of Mg metal at the source temperature of
16 2200 K is significantly higher (10^7 Pa in order of magnitude) than partial pressure of O_2
17 (3.0×10^2 Pa), However, Mg powder may evaporate in thermally disequilibrium.
18 Rapidly evaporated Mg vapors will be oxidized by fresh oxygen supplied by thermal

convection from the bottom of the evaporation source. We can find no significant increase of relative intensity at 17 μm band caused by Mg-O to the 10 μm band caused by Si-O from 1 cm to 10 cm in Fig. 2. In addition, there are no magnesium metal particles during TEM observation and the morphology of MgO particles produced as a byproduct was completely cubic, which is characteristic shape of a particle with NaCl-type structure, suggesting direct nucleation of MgO from vapor. If Mg particles oxidize during convection, the morphology will be flower like and excess of 17 μm band will appear as height increases. According to Hallenbeck et al., (2000), peak wavelength attributable to Si-O stretching mode in a silicate shifts from 9.3 μm to 9.7 μm after sufficient reduction/oxidation reaction in an annealing process. In present study, corresponding peak wavelength measured at 1 cm from the evaporation source at 9.7 μm indicates that oxidation is almost completed at gas phase or just after nucleation. Therefore, it seems that oxidation has almost completed at 1 cm from the evaporation source. If the composition of just nucleated particles is insufficient in oxygen from forsterite composition (Mg_2SiO_4), it can be oxidized in the convection, but not only higher than 6 cm but also in 1-6 cm above the evaporation source. Though we cannot completely exclude the possibility that oxidation induces the crystallization in 500 K atmosphere, the effect will not be significant.

Thirdly, amorphous particles might be able to crystallize by thermal annealing. The atmospheric temperature at various distances from an evaporation source at various temperatures under a total pressure of about 1.0×10^4 Pa has already been reported (Kaito 1991; Kaito 2006; Kimura et al., 2011b). Figure 5 shows a summary of the temperature distribution as a distance from the evaporation source. The temperature of the particles can be regarded as identical to that of the gas, because the cooling rate of the particles is two orders of magnitudes faster than that of the gas (Appendix 1). Therefore, the crystallization temperature at 6–10 cm above the evaporation source can be estimated to be about 500 K or less. The temperature of crystallization of amorphous Mg-bearing silicate to form forsterite is more than 500 K lower than that for crystallization by thermal annealing [~1000 K; Hallenbeck (2000) Koike et al. (2010)]. On the KBr methods, the IR spectra of the samples collected from 10.5 and 18 cm above the evaporation source did not show significant difference in the relative intensity between the double bands of forsterite. Therefore, further crystallization of the samples is insignificant after 10 cm and the radiation heating from the hot evaporation source can also be negligible because of relatively short experimental duration. From this estimation, we conclude that significant crystallization occurred at around 6–10 cm during free-flying in our experiments without thermal heating.

Fourthly, secondary nucleation from molten particles will be discussed. Metastable particles preferentially nucleate prior than stable crystalline phase, such as liquid droplets or amorphous structures, because of the advantage of the lower surface free energy of metastable phases than that of crystalline phase; this preference is known as Ostwald's step rule (Ostwald, 1897). Nagashima et al. (2006) reported that crystallization from a free-flying melt with ~1 mm in diameter of forsterite composition is difficult to occur compared to that from a forsterite melt in a crucible, which provides its surface as a nucleation cite of crystals, and was observed at a supercooling of ΔT = 1000 K. The condensed warmed particles in our experiment cooled and crystallized in a similar manner to crystallization from a free-flying melt with a forsterite composition. The activation energy of crystallization from a silicate droplet (E_{liq}/k = 23000 K) is significantly lower than that from the amorphous material (E_{amo}/k = 39000 K; Tanaka et al., 2008; Tanaka et al., 2010). These results suggest that our sample underwent crystallization from the melt rather than annealing of amorphous condensates. In the initial stages of nucleation, each nucleus consists of a countable number of molecules. Then, the melting temperature is significantly lower than that of the bulk material (Lee et al., 2009). In addition, the molecules in nanoparticles diffuse much faster in their body than those in the bulk material (e.g., Yasuda et al., 1992). These characteristic

phenomena in nano-scale can regard particles being droplets. In consequence, we suggest that low temperature crystallization occurred from supercooled liquid droplets and was enabled by considerably reduced activation energy for crystallization in nano droplets.

6. ASTRONOMICAL IMPLICATIONS

Normalized IR spectra of typical AGB stars with a silicate 10-μm feature (Speck et al., 2000) are compared with our result in Fig. 6. The IR spectrum of the initial condensates before crystallization [Fig. 2(a)] reproduces the features of the "classical" narrowest silicate feature observed around evolved stars at 9.7 μm, including the peak position and the FWHM.

The astronomically observed feature at 9.7 μm arising from warm non-crystalline silicate is reproduced simultaneously by nanometer-sized particles in our experiment. Size effects of nanoparticles lead to nucleation as liquid droplets in our experiment. Nuclei of silicate should therefore be considered as a molten rather than an amorphous material at least in our experimental condition. In particular, nucleation as liquid droplets is significant for the crystallization. This result gives us a brand new picture of silicate crystallization from nanodroplet, which might be occurred in relatively higher

vapor pressure environment in dust formation region.

7. CONCLUSIONS

We have investigated a new, in-situ, IR technique for performing measurements on free-flying nucleating nanoparticles, which we named the *Free-flying In-situ infrared measurement of Nucleating nanoparticles Experimental (FINE)* system. This technique is free of KBr-embedding effects, and therefore permits direct comparisons to be made with astronomical observations. By using the FINE system, we were able to monitor the nucleation and subsequent growth of silicate nanoparticles *in situ*. These studies showed that size effects of nanoparticles lead to nucleation as droplets and subsequent crystallization at a relatively low temperature (<500 K) in our experiments. The 9.7-μm feature of astronomical silicate was well reproduced by the FINE system.

ACKNOWLEDGMENTS

The authors thank Joseph A. Nuth III of NASA/GSFC for valuable comments. This work was supported by a Grant-in-Aid for Challenging Exploratory Research from KAKENHI (22654022) and by a Grant-in-Aid for Young Scientists (A) from KAKENHI (24684033).

REFERENCES

Bohren, C. F., & Huffman, D. R. 1983, Absorption and Scattering of Light by Small Particles (New York: Wiley)

Bouwman, J., Meeus, G., de Koter, A., et al. 2001, A&A, 375, 950

Fabian, D., Henning, T., Jäger, C., et al. 2001, A&A, 378, 228

Hallenbeck, S. L., Nuth, J. A., III, & Nelson, R. N., 2000, ApJ, 535, 247

Hanner, M. S., Lynch, D. K., & Russell, R. W. 1994, ApJ, 425, 274

Honda, M., Kataza, H., Okamoto, K. Y., Yamashita, T., et al. 2006, ApJ, 646, 1024Jäger, C., Molster, F., Dorschner, J., et al. 1998, A&A, 339, 904

Jones, O. C., Kemper, F., Sargent, B. A., McDonald, I., et al. 2012, Astron. Soc, 427, 3209

Kaito, C. 1991, Kemuri no Himitsu (Tokyo: Kyohritsu) (in Japanese)

Kaito, C. 2006, J. Plasma Res. 82, 2, 87

Kimura, Y., Miyazaki, Y., Kumamoto, A., Saito, M., & Kaito, C. 2008, ApJ, 680, L89

Kimura, Y. & Nuth, J. A., III. 2009, ApJL, 697, L10

Kimura, Y., Nuth, J. A., III., Tsukamoto, K. & Kaito, C. 2011a, Meteoritics & Planetary Science, 46, 92

Kimura, Y., & Tsukamoto, K., 2011b, J. Japan Soc. Microgravity Appl., 28, 2, S19

Kimura, Y., Miura, H., Tsukamoto, K., Li, C., & Maki, T. 2011c, Journal of Crystal Growth, 316, 196

Koike, C., Imai, Y., Chihara, H., et al. 2010, ApJ, 709, 983

Lee, J., Tanaka, T., & Mori, H. 2009, Nanotechnology, 20, 475706

Molster, F., Waters, L.B.F.M., Tielens, A.G.G.M. & Barlow, M.J. 2002, A&A, 382, 184

Molster, F., & Kemper, C. 2005, Space Sci. Rev., 119, 3

Murata, K., Takakura, T., Chihara, H., et al. 2009, ApJ, 696, 1612

Mutschke, H. 2013, in The Life Cycle of Dust in the Universe: Observations, Theory, and Laboratory Experiments, Pos (LCDU 2013) 042, http://pos.sissa.it/archive/conferences/207/042/LCDU%202013_042.pdf

Min, M., Waters, L. B. F. M., de Koter, A., et al. 2007, A&A, 333, 188

Nagashima, K., Tsukamoto, K., Satoh, H., et al. 2006, J. Cryst. Growth, 293, 1, 193

Ostwald, W. 1897, Z. Phys. Chem., 22, 289–330

Speck, A. K., Barlow,M. J., Sylvester, R. J., & Hofmeister, A.M. 2000, A&AS,146, 437

Tamanai, A., Mutschke, H., Blum, J., & Meeus, G. 2006, ApJ, 648, L147

Tanaka, K. K., Yamamoto, T. & Miura, H., 2010, ApJ, 717, 586

Tanaka, K. K., Yamamoto, T., Nagashima, K., & Tsukamoto, K. 2008, J. Cryst. Growth, 310, 1281

1 Tsuchiyama, A. 1998, Mineral. J., 20, 59

2 van Boekel, R., Min, M., Waters, L. B. F. M., de Koter, A., et al. 2005, A&A, 437, 189

3 Watanabe, J., Honda, M., Ishiguro, M., Ootsubo, T., et al. 2009, Astron. Soc. Japan, 61,

4 679

5 Waters, L. B. F. M., Molster, F. J., de Jong, T., et al., 1996, A&A, 315, L361.

6 Yasuda, H., Mori, H., Komatsu, M., et al. 1992, J. Electron Microsc., 41, 267

7

8

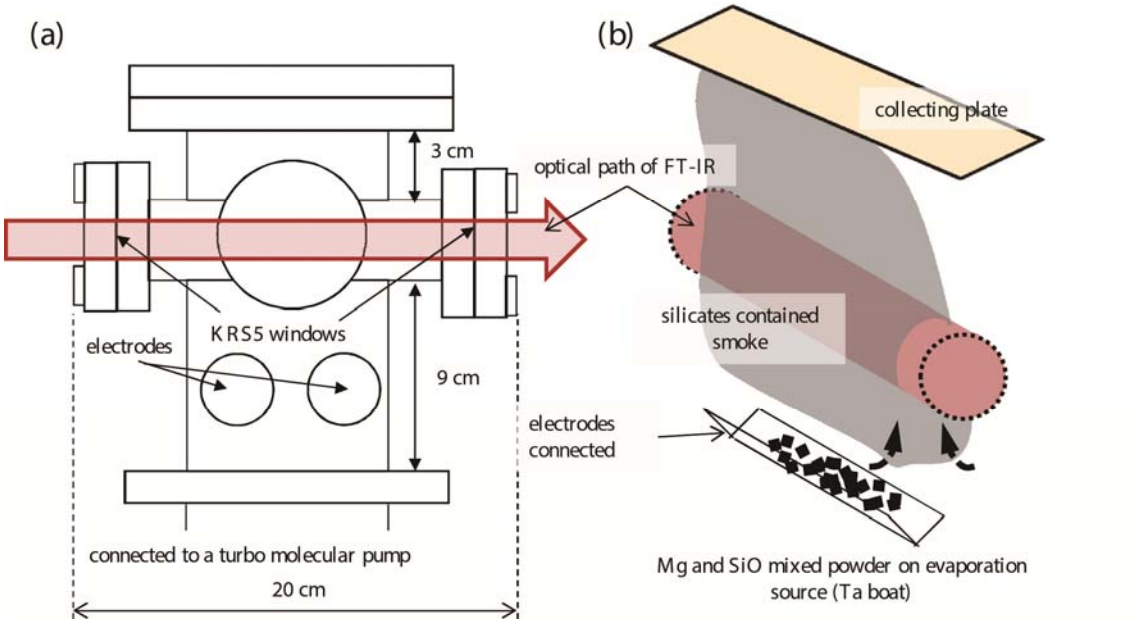

Figure 1. Schematics showing the FINE system. (a) Outside view of the chamber, the bottom of which is connected to a high-vacuum pumping system for evacuation. The large arrow shows the optical path for FT-IR. (b) Inside image during experiments. The gray area indicates the smoke consisting of nanoparticles. The dotted arrows show gas convection generated by the hot evaporation source, a V-shaped tantalum plate. The collecting holder is located 10.5 cm above the evaporation source.

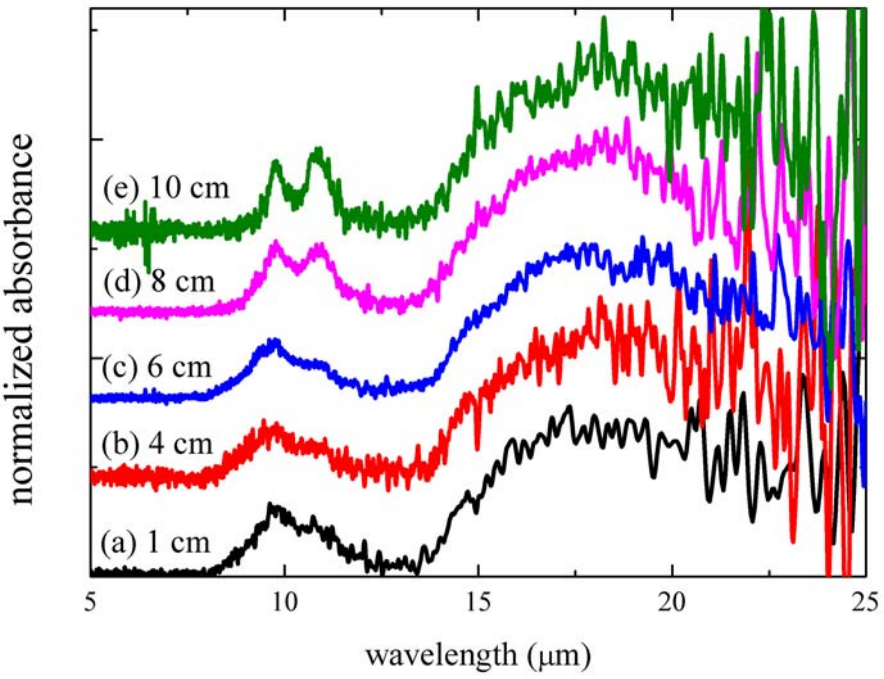

Figure 2. Representative spectra recorded at various heights above the source, maintained at 2200±200 K, are shown. Normalized spectra (from the bottom to the top) correspond to measurements taken at 1, 4, 6, 8 and 10 cm, respectively, over the range of wavelengths from 5 to 25 μm. The 10-μm feature and the 17-μm feature are attributable to silicates and MgO, respectively. The lower S/N ratios at wavelengths longer than 20 μm are the result of lower sensitivity of the detector.

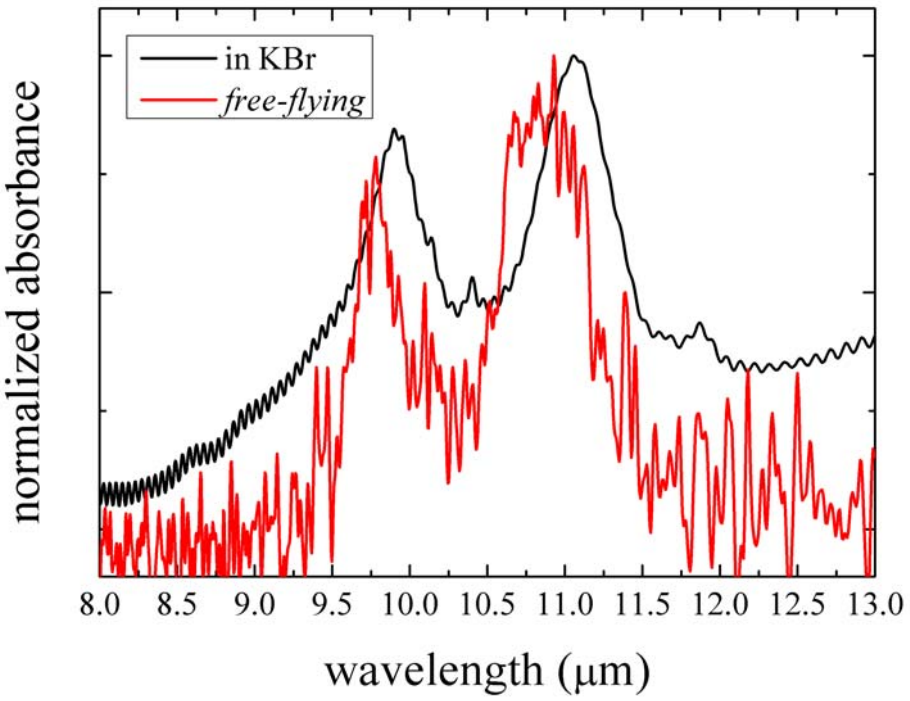

Figure 3. FT-IR spectra of free-flying silicate nanoparticles at 10 cm from the evaporation source (red line) and of collected silicate nanoparticles deposited on a collecting holder fixed 10.5 cm above the evaporation source and subsequently embedded in a KBr pellet (black line). The peak wavelength and width were altered as a result of embedding in KBr.

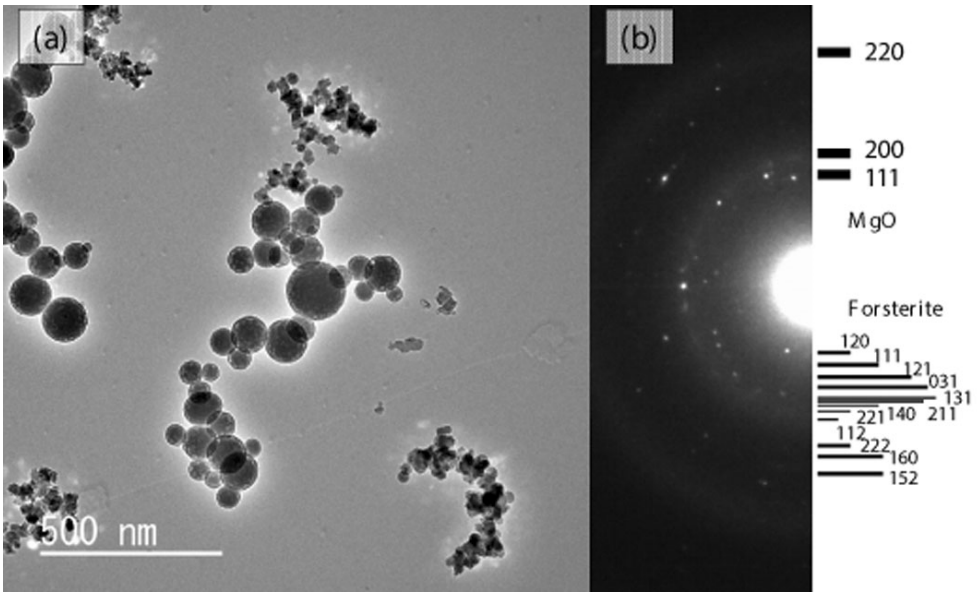

Figure 4. Bright-field TEM image and the corresponding electron-diffraction pattern of condensates. Spherical particles containing forsterite crystals and cubic-shaped MgO were observed

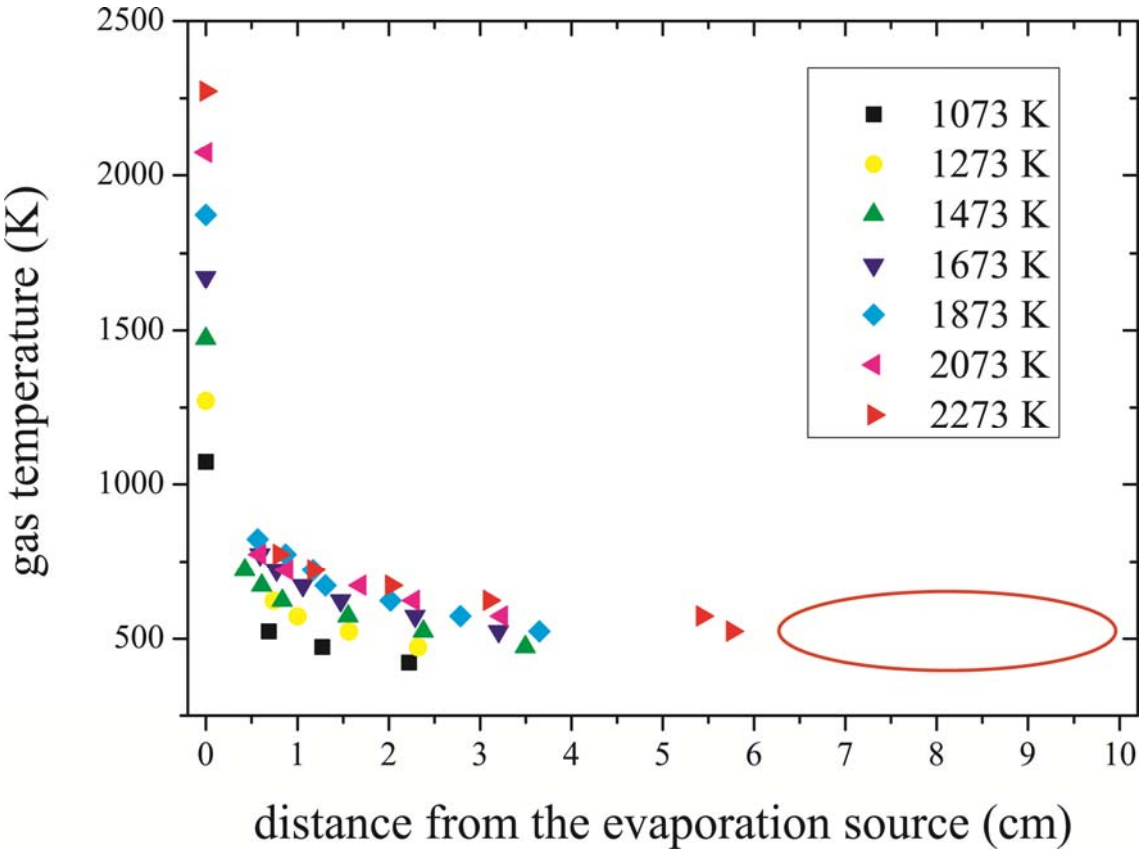

Figure 5. Temperature distributions in the vertical direction of the gas atmosphere above the evaporation source maintained at various temperatures. The temperature at 0 cm is the temperature of the source, as measured by using a pyrometer; the other temperatures at various heights were measured by using a thermocouple (Kaito. 1991; Kaito. 2006). The yellow triangle markers correspond to the temperature in this work. The red circle indicates the expected temperature range in which crystallization is likely to have occurred.

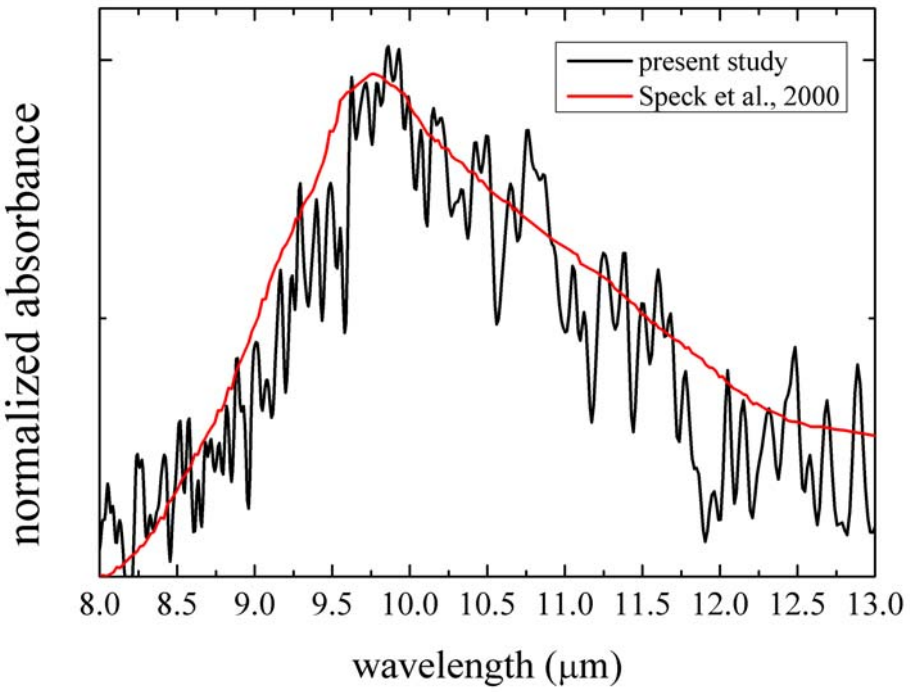

Figure 6. Direct comparison of astronomical observations and observations on free-flying silicates made in this study. Broad silicate 9.7-μm band, classified as group *A* according to Speck et al. 2000 (thick line) and initial condensates measured at 1 cm above the evaporation source (thin line).

Appendix 1

In the setup for our experiments, the cooling timescale for particles is determined by collision with ambient Ar gas, and is given by the following expression:

$$\tau_{cool,Pa} = \frac{2\rho_d c_p r}{3nk\bar{v}}$$

This assumes that the temperature of the particles is sufficiently greater than that of the ambient gas (Tanaka et al., 2010). Here, ρ_d (~3.0 g cm^{-3}) is the mean density of the particles, c_p (1.9×10^7 erg g^{-1} K^{-1}) is the specific heat of the silicate melt (Navrtosky 1995), r (50 nm) is the radius of the particles obtained by TEM observation, n is the number density of the ambient gas under an atmosphere of 1.0×10^4 Pa, k is the Boltzmann constant, and $\bar{v}$ is the thermal velocity calculated from the gas temperature. We can now evaluate the cooling timescale $\tau_{cool,Pa} \approx 1 \times 10^{-5}$ s at a gas temperature of 500 K; this is shorter than cooling timescale of the ambient gas $\tau_{coolGas} \approx 1 \times 10^{-1}$ s calculated from the mean rising air current, which is of the order of 15 cm s^{-1}. Therefore, the temperature of the particles is the same as that of the ambient gas.

References

Navrotsky, A. 1995, in Mineral Physics and Crystallography, Handbook of Physical Constants, ed. T. J. Ahrens (Washington, DC: AGU), 18